Data report: gas isotope and conversion ratio of headspace and void gas, IODP Expedition 344[1]

Jiyoung Choi,[2] Ji-Hoon Kim,[2] Gil-Young Kim,[2] Se-Won Chang[2]

Chapter contents

Abstract 1
Introduction 1
Methods and materials 1
Results 2
Conclusion 3
Acknowledgments 3
References 3
Figures 5
Tables 9

[1] Choi, J., Kim, J.-H., Kim, G.-Y., and Chang, S.-W., 2016. Data report: gas isotope and conversion ratio of headspace and void gas, IODP Expedition 344. *In* Harris, R.N., Sakaguchi, A., Petronotis, K., and the Expedition 344 Scientists, *Proceedings of the Integrated Ocean Drilling Program,* 344: College Station, TX (Integrated Ocean Drilling Program). doi:10.2204/iodp.proc.344.203.2016
[2] Petroleum and Marine Research Division, Korea Institute of Geoscience and Mineral Resources, 124 Gwahang-no, Yuseong-gu, Daejeon 34132, Republic of Korea. Correspondence author: jychoi@kigam.re.kr

Abstract

Gas stable isotopes ($\delta^{13}C_{CH4}$, δD_{CH4}, and $\delta^{13}C_{CO2}$) and the conversion ratios of headspace gas and void gas have been analyzed at Integrated Ocean Drilling Program Expedition 344 Sites U1380, U1412, and U1413 to reveal the origin and migration of gas. The results of headspace gas and void gas analyses illustrate that methane (C_1) is the dominant component and ethane (C_2) is a minor component. Variations in C_1/C_{2+} ratios with depth display differing trends across sites. The $\delta^{13}C_{CH4}$ and δD_{CH4} values are less than –57.0‰ and –181‰, respectively, indicating that hydrocarbon gas might be originated through CO_2 reduction. In addition, the organic matter to hydrocarbon gas conversion ratios of biogenic void gas at Sites U1412 and U1413 range from 22% to 30%.

Introduction

The Costa Rica Seismogenesis Project, Program A Stage 2, drilled at five sites located offshore of the Osa Peninsula near the incoming Cocos Ridge to study the processes controlling earthquakes in an erosional subduction zone (see the **"Expedition 344 summary"** chapter [Harris et al., 2013a]). Among the five sites, Sites U1380, U1412, and U1413 were studied to investigate deep fluid transportation. Several studies on the sources and evolution of the magmas are well advanced, even though subduction zone settings can be quite complex (e.g., Stern, 2002; van Keken, 2003; Hall and Kincaid, 2001). In contrast, we know little about fluid migration in subduction zones. The characterization of gas isotope and conversion ratio in headspace gas (HS) and void gas (VG) could help to understand deep fluid systems and the origin of gases. In this study, we provide the molecular and stable isotopic compositions of HS and VG, which are indicators for the origin and migration of the gases. Furthermore, we show the organic matter to hydrocarbon gas conversion ratios at the drilled sites.

Methods and materials

Gas composition

The HS samples were analyzed onboard by an Agilent 6890 Series II gas chromatograph (GC3) (see the **"Methods"** chapter [Harris

doi:10.2204/iodp.proc.344.203.2016

et al., 2013b]). The VG samples were analyzed onshore by an Agilent 7890A gas chromatograph with a flame ionization detector and a thermal conductivity detector at Korea Institute of Geoscience and Mineral Resources (KIGAM).

Isotope analysis

A total of 43 HS samples from Sites U1380, U1412, and U1413 and 27 VG samples from Sites U1412 and U1413 were used for the gas isotopic analyses. The carbon ($\delta^{13}C_{CH4}$ and $\delta^{13}C_{CO2}$) and hydrogen (δD_{CH4}) stable isotopic ratios of the gases were analyzed using an isotope ratio–monitoring gas chromatograph/mass spectrometer at Isotech, Champaign, IL. All isotopes are reported in the usual δ notation relative to Vienna Pee Dee Belemnite (V-PDB) for carbon and Vienna Standard Mean Ocean Water (V-SMOW) for hydrogen:

$$\delta(‰) = [(R_{sample} - R_{standard})/R_{standard}] \times 1000,$$

where R represents the $^{13}C/^{12}C$ ratio and D/H of the sample and standard for each isotope. The analytical reproducibility was ±0.1‰ for $\delta^{13}C$ and ±2‰ for δD.

Conversion ratio

The conversion ratio was calculated using the Rayleigh ratio (modified from Pohlman et al., 2009).

$$\delta^{13}C_{CO2,t} = \delta^{13}C_{CO2,i} - \varepsilon_c \ln(f)$$

$$\delta^{13}C_{CH4,t} = \delta^{13}C_{CO2,i} - \varepsilon_c[1 + \ln(f)]$$

where

$\delta^{13}C_{CO2,t}$ = isotopic ratio of CO_2 at time t,
$\delta^{13}C_{CH4,t}$ = isotopic ratio of CH_4 at time t,
$\delta^{13}C_{CO2,i}$ = isotopic ratio of sedimentary organic matter at depth i,
ε_c = fractionation factor, and
$\ln(f)$ = remaining fraction of the initial substrate.

The model determines that the proportion of methane is produced by in situ methanogenesis.

Results

Headspace gas

The HS analysis results show that methane is a major component and ethane a minor component at all sites (see the **"Expedition 344 summary"** chapter [Harris et al., 2013a]) (Table **T1;** Fig. **F1**). Methane concentration is relatively constant with depth at Sites U1380, U1412, and U1413. Ethane concentration does not show vertical variation with depth at Site U1380, whereas it increases with depth at Sites U1412 and U1413. In general, C_1/C_{2+} ratios are >1000 in biogenic gases and <300 in thermogenic gases (Claypool and Kvenvolden, 1983; Whiticar et al., 1986; Whiticar, 1999; Milkov et al., 2005; Pape et al., 2010; Kim et al., 2011, 2012). In this study, the C_1/C_{2+} ratio is lowest (<300) in lithostratigraphic Unit I at Site U1380 and Unit III at Site U1413.

The $\delta^{13}C_{CH4}$ and δD_{CH4} values of biogenic methane typically range from –110‰ to –50‰ and –400‰ to –100‰, respectively, whereas those of thermogenic methane range from –50‰ to –20‰ and –275‰ to –50‰, respectively (Whiticar, 1999). In this study, $\delta^{13}C_{CH4}$ and δD_{CH4} values range from –64.5‰ to –57.7‰ and –210‰ to –187‰, respectively, at Site U1380; from –81.3‰ to –57.0‰ and –194‰ to –185‰, respectively, at Site U1412; and from –71.7‰ to –58.2‰ and –209‰ to –181‰, respectively, at Site U1413. The lowest values of $\delta^{13}C_{CH4}$ (approximately –80‰) are found in the upper part of Site U1412 (Fig. **F1;** Table **T1**). This interval contains a sulfate methane transition zone (see the **"Expedition 344 summary"** chapter [Harris et al., 2013a]). The $\delta^{13}C_{CH4}$ values are constant with depth except in the upper part at Site U1412. Crossplots of $\delta^{13}C_{CH4}$ versus C_1/C_{2+} and $\delta^{13}C_{CH4}$ versus δD_{CH4} illustrate that most analyzed data are located in the field of biogenic methane generated by CO_2 reduction (Fig. **F2**).

Void gas

The VG analysis results also show that methane is a major component and ethane is a minor component at all sites (see the **"Expedition 344 summary"** chapter [Harris et al., 2013a]) (Table **T2;** Fig. **F3**). Methane concentration is relatively constant with depth at Sites U1412 and U1413. Ethane concentrations increase with depth at Sites U1412 and U1413. Ethane concentrations at Site U1412 (average = 41 ppmv) are greater than those at Site U1413 (average = 6 ppmv).

The $\delta^{13}C_{CH4}$ and δD_{CH4} values vary from –74.9‰ to –64.3‰ and –193‰ to –183‰, respectively, at Site U1412 and from –73.0‰ to –71.3‰ and –187‰ to –183‰, respectively, at Site U1413. The $\delta^{13}C_{CO2}$ values range from –10.8‰ to 1.4‰ at Site U1412 and from –3.8‰ to 0.5‰ at Site U1413, indicating a decrease with depth (Fig. **F3;** Table **T2**). Crossplots of $\delta^{13}C_{CH4}$ versus C_1/C_{2+}, $\delta^{13}C_{CH4}$ versus δD_{CH4}, and

$\delta^{13}C_{CH4}$ versus $\delta^{13}C_{CO2}$ indicate that the gas is generated by CO_2 reduction (Fig. F4).

Conversion ratio

We calculate how much organic matter should convert to hydrocarbon gas in situ using the Rayleigh ratio based on the carbon stable isotopic data for organic matter and VG (modified from Pohlman et al., 2009) (Table T2; Fig. F3). Carbon stable isotopes of organic matter are between –25.0‰ and –23.5‰ at Site U1412 and between –26.0‰ and –23.6‰ at Site U1413 (see the "Expedition 344 summary" chapter [Harris et al., 2013a]). Estimated conversion ratios vary between 21.8% and 30.7% at Site U1412 and between 26.4% and 30.2% at Site U1413, slightly decreasing with depth (Fig. F3).

Conclusion

1. Methane dominates the composition of both HS and VG. The origin of methane is primarily biogenic.
2. The C and H isotopes of most HS and VG indicate that the gas was generated by CO_2 reduction.
3. Conversion ratios of biogenic VG at Sites U1412 and U1413 range from 22% to 30%.

Acknowledgments

This study used samples provided by the Integrated Ocean Drilling Program (IODP) and was financially supported by Korea International Ocean Discovery Program (K-IODP) of Ministry of Oceans and Fisheries (MOF).

References

Claypool, G.E., and Kvenvolden, K.A., 1983. Methane and other hydrocarbon gases in marine sediment. *Annual Review of Earth and Planetary Sciences,* 11(1):299–327. http://dx.doi.org/10.1146/annurev.ea.11.050183.001503

Hall, P.S., and Kincaid, C., 2001. Diapiric flow at subduction zones: a recipe for rapid transport. *Science*, 292(5526):2472–2475. http://dx.doi.org/10.1126/science.1060488

Harris, R.N., Sakaguchi, A., Petronotis, K., Baxter, A.T., Berg, R., Burkett, A., Charpentier, D., Choi, J., Diz Ferreiro, P., Hamahashi, M., Hashimoto, Y., Heydolph, K., Jovane, L., Kastner, M., Kurz, W., Kutterolf, S.O., Li, Y., Malinverno, A., Martin, K.M., Millan, C., Nascimento, D.B., Saito, S., Sandoval Gutierrez, M.I., Screaton, E.J., Smith-Duque, C.E., Solomon, E.A., Straub, S.M., Tanikawa, W., Torres, M.E., Uchimura, H., Vannucchi, P., Yamamoto, Y., Yan, Q., and Zhao, X., 2013a. Expedition 344 summary. *In* Harris, R.N., Sakaguchi, A., Petronotis, K., and the Expedition 344 Scientists, *Proceedings of the Integrated Ocean Drilling Program,* 344: College Station, TX (Integrated Ocean Drilling Program). http://dx.doi.org/10.2204/iodp.proc.344.101.2013

Harris, R.N., Sakaguchi, A., Petronotis, K., Baxter, A.T., Berg, R., Burkett, A., Charpentier, D., Choi, J., Diz Ferreiro, P., Hamahashi, M., Hashimoto, Y., Heydolph, K., Jovane, L., Kastner, M., Kurz, W., Kutterolf, S.O., Li, Y., Malinverno, A., Martin, K.M., Millan, C., Nascimento, D.B., Saito, S., Sandoval Gutierrez, M.I., Screaton, E.J., Smith-Duque, C.E., Solomon, E.A., Straub, S.M., Tanikawa, W., Torres, M.E., Uchimura, H., Vannucchi, P., Yamamoto, Y., Yan, Q., and Zhao, X., 2013b. Methods. *In* Harris, R.N., Sakaguchi, A., Petronotis, K., and the Expedition 344 Scientists, *Proceedings of the Integrated Ocean Drilling Program,* 344: College Station, TX (Integrated Ocean Drilling Program). http://dx.doi.org/10.2204/iodp.proc.344.102.2013

Kim, J.-H., Park, M.-H., Chun, J.-H., and Lee, J.Y., 2011. Molecular and isotopic signatures in sediments and gas hydrate of the central/southwestern Ulleung Basin: high alkalinity escape fuelled by biogenically sourced methane. *Geo-Marine Letters*, 31(1):37–49. http://dx.doi.org/10.1007/s00367-010-0214-y

Kim, J.-H., Torres, M.E., Choi, J., Bahk, J.-J., Park, M.-H., and Hong, W.-L., 2012. Inferences on gas transport based on molecular and isotopic signatures of gases at acoustic chimneys and background sites in the Ulleung Basin. *Organic Geochemistry*, 43:26–38. http://dx.doi.org/10.1016/j.orggeochem.2011.11.004

Milkov, A.V., Claypool, G.E., Lee, Y.-J., and Sassen, R., 2005. Gas hydrate systems at Hydrate Ridge offshore Oregon inferred from molecular and isotopic properties of gas hydrate-bound and void gases. *Geochimica et Cosmochimica Acta,* 69(4):1007–1026. http://dx.doi.org/10.1016/j.gca.2004.08.021

Pape, T., Bahr, A., Rethemeyer, J., Kessler, J.D., Sahling, H., Hinrichs, K.-U., Klapp, S.A., Reeburgh, W.S., and Bohrmann, G., 2010. Molecular and isotopic partitioning of low-molecular-weight hydrocarbons during migration and gas hydrate precipitation in deposits of a high-flux seepage site. *Chemical Geology*, 269(3–4):350–363. http://dx.doi.org/10.1016/j.chemgeo.2009.10.009

Pohlman, J.W., Kaneko, M., Heuer, V.B., Coffin, R.B., and Whiticar, M., 2009. Methane sources and production in the northern Cascadia margin gas hydrate system. *Earth and Planetary Science Letters,* 287(3–4):504–512. http://dx.doi.org/10.1016/j.epsl.2009.08.037

Stern, R.J., 2002. Subduction zones. *Reviews of Geophysics,* 40(4):1–38. http://dx.doi.org/10.1029/2001RG000108

van Keken, P.E., 2003. The structure and dynamics of the mantle wedge. *Earth and Planetary Science Letters,* 215(3–4):323–338. http://dx.doi.org/10.1016/S0012-821X(03)00460-6

Whiticar, M.J., Faber, E., and Schoell, M., 1986. Biogenic methane formation in marine and freshwater environments: CO_2 reduction vs. acetate fermentation—isotope evidence. *Geochimica et Cosmochimica Acta,* 50(5):693–709. http://dx.doi.org/10.1016/0016-7037(86)90346-7

Whiticar, M.J., 1999. Carbon and hydrogen isotope systematics of bacterial formation and oxidation of methane. *Chemical Geology,* 161(1–3):291–314. http://dx.doi.org/10.1016/S0009-2541(99)00092-3

Initial receipt: 9 August 2015
Acceptance: 15 March2016
Publication: 11 May 2016
MS 344-203

Figure F1. Downcore profiles of methane and ethane concentration, C_1/C_{2+} ratios, and isotopic compositions ($\delta^{13}C_{CH4}$ and δD_{CH4}) in headspace gas at (**A**) Site U1380, (**B**) Site U1412, and (**C**) Site U1413. Red dashed lines represent lithostratigraphic unit boundaries. Methane and ethane concentration and C_1/C_{2+} ratios are onboard data.

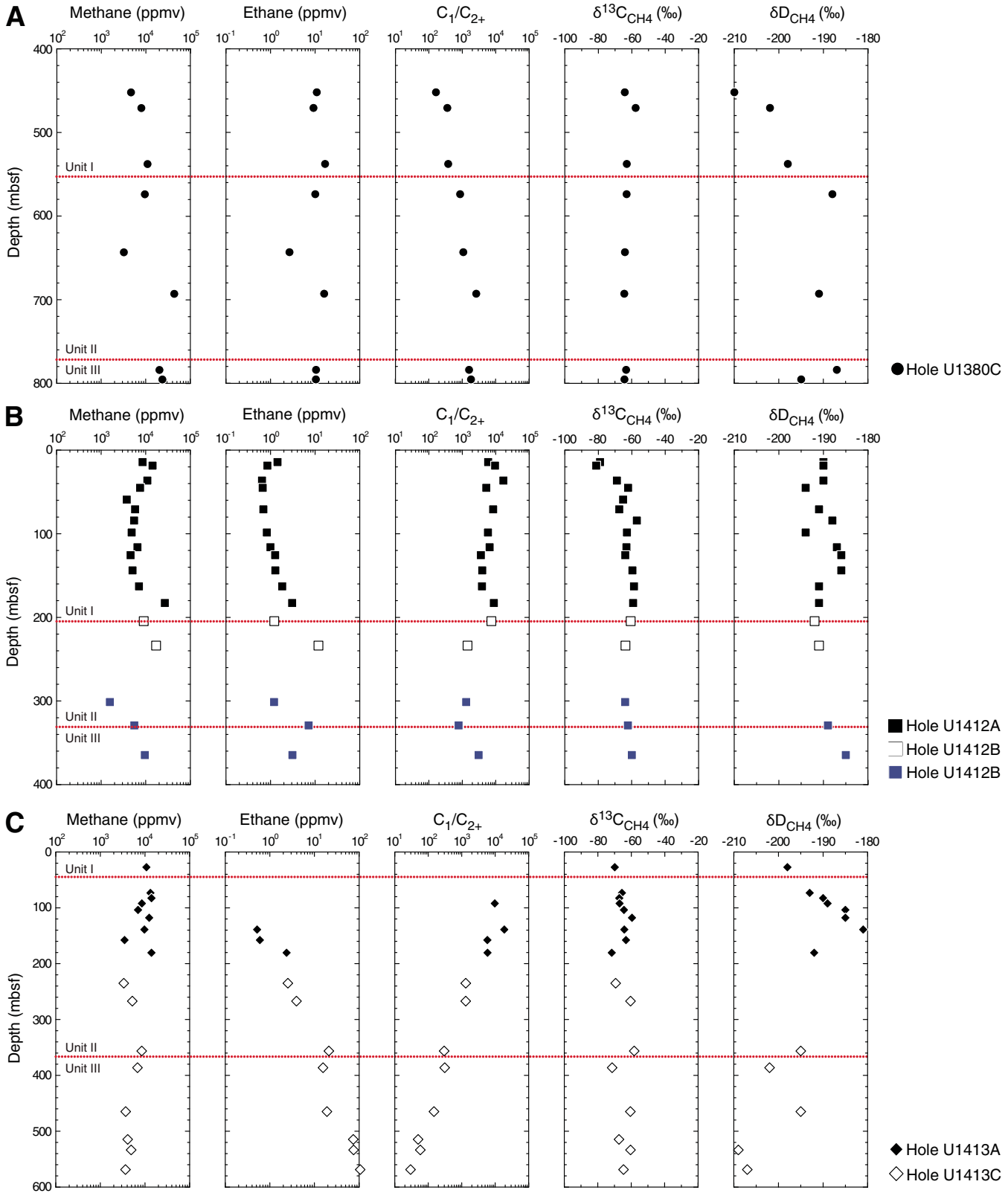

Figure F2. (**A**) Relationship between C_1/C_{2+} ratios and $\delta^{13}C_{CH4}$ values (modified from Bernard et al., 1978) and (**B**) $\delta^{13}C_{CH4}$ versus δD_{CH4} (adapted from Whiticar, 1999) in headspace gas at Sites U1380, U1412, and U1413.

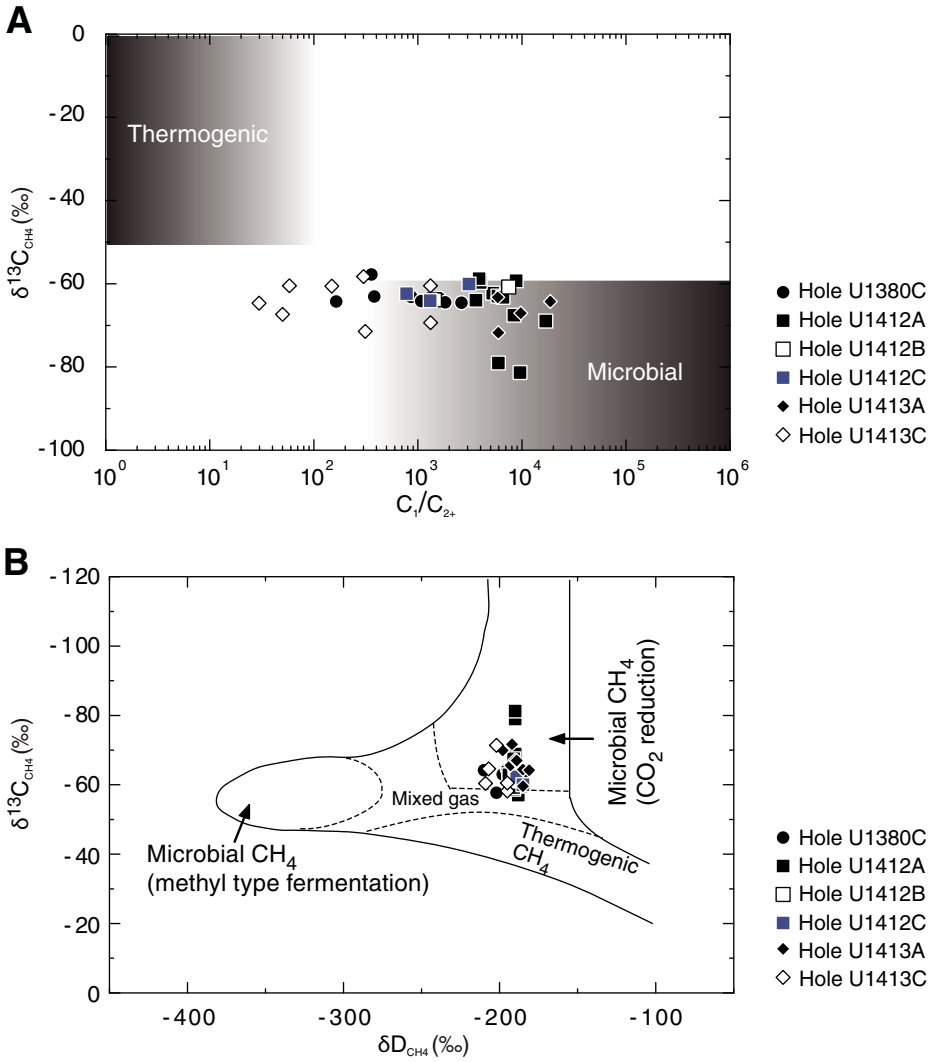

Figure F3. Downcore profiles of methane and ethane concentration, C_1/C_{2+} ratios, isotopic compositions ($\delta^{13}C_{CH4}$, δD_{CH4}, and $\delta^{13}C_{CO2}$), and conversion ratio in void gas at (**A**) Site U1412 and (**B**) Site U1413. Red dashed lines represent lithostratigraphic unit boundaries. Methane and ethane concentration and C_1/C_{2+} ratios are onboard data.

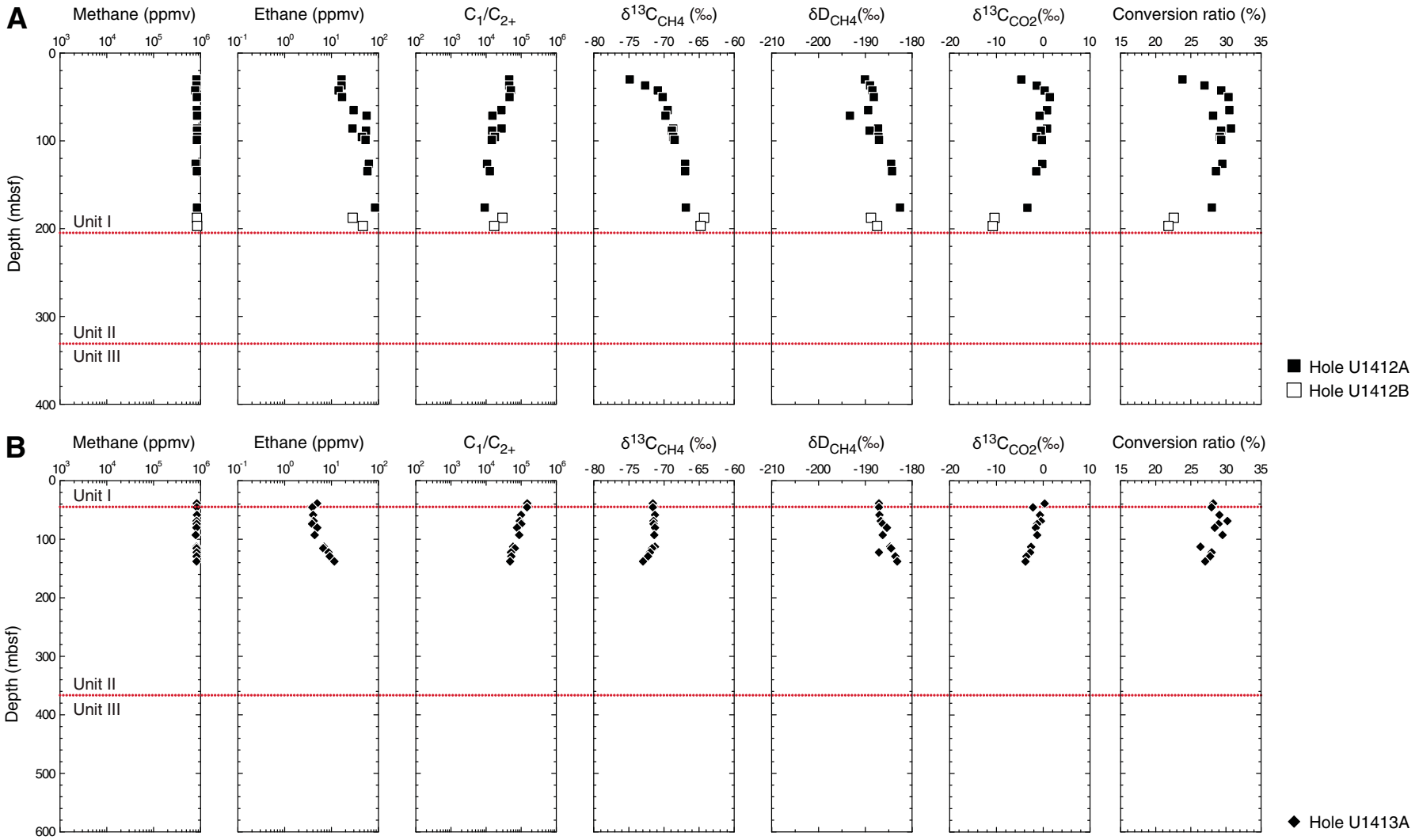

Figure F4. A. Relationship between the C_1/C_{2+} ratios and $\delta^{13}C_{CH4}$ values (modified from Bernard et al., 1978). **B.** $\delta^{13}C_{CH4}$ versus δD_{CH4} (adapted from Whiticar, 1999). **C.** $\delta^{13}C_{CH4}$ versus $\delta^{13}C_{CO2}$ (adapted from Whiticar, 1999; Pohlman et al., 2009; Kim et al., 2012) in void gas at Sites U1412 and U1413.

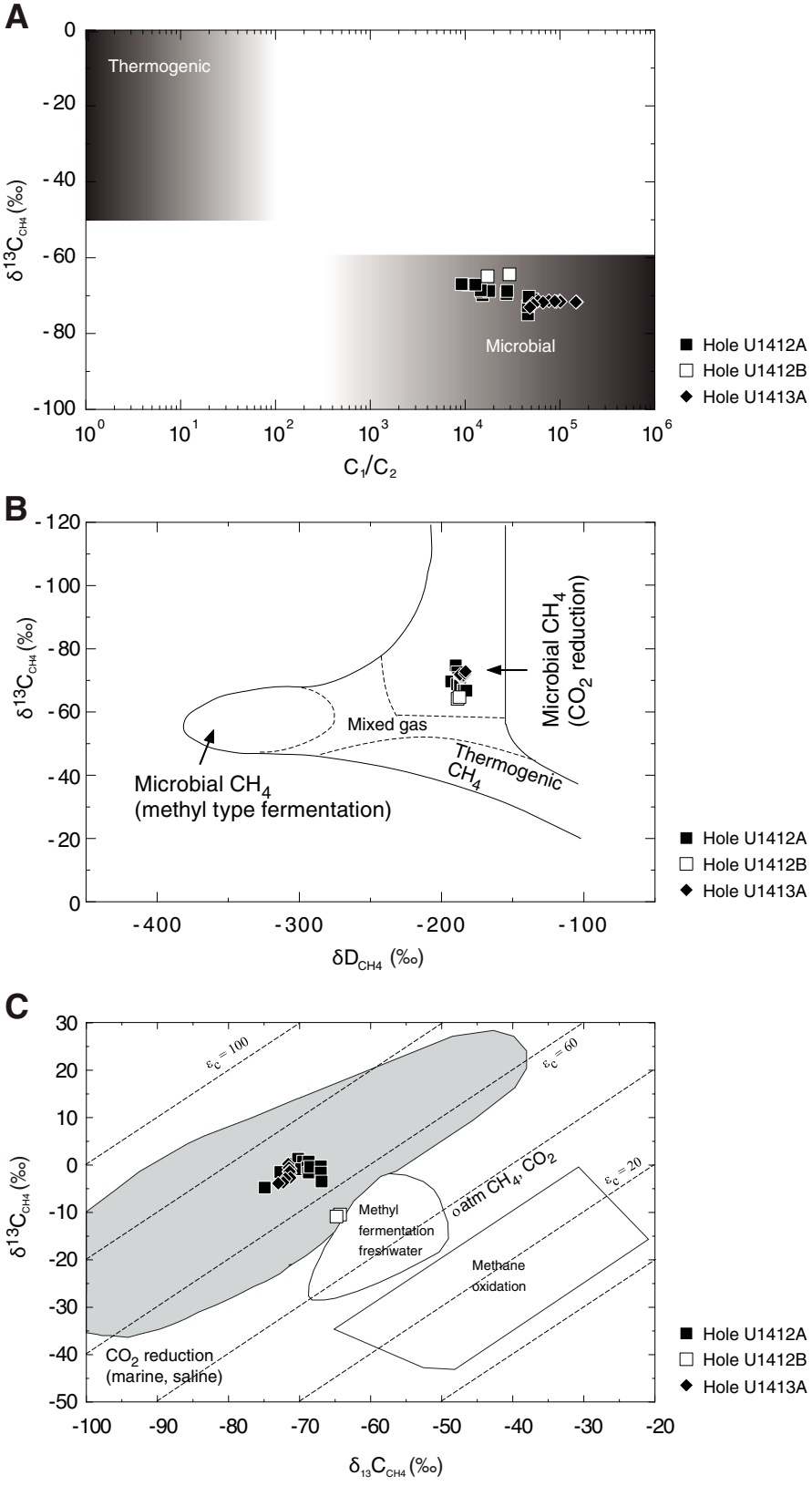

Table T1. Molecular and isotopic compositions of headspace gas, Sites U1380, U1412, and U1413.

Core, section, interval (cm)	Depth (mbsf)	Methane (ppmv)	Ethane (ppmv)	C_1/C_{2+}	$\delta^{13}C_{CH4}$ (‰)	δD_{CH4} (‰)
344-U1380C-						
3R-4, 0–5	451.94	4,629	10.9	163	–64.2	–210
5R-4, 0–5	470.67	7,901	9.2	356	–57.7	–202
12R-3, 0–5	537.63	10,859	16.8	379	–63.0	–198
16R-1, 0–5	573.80	9,464	10.1	860	–63.1	–188
23R-2, 0–5	643.17	3,199	2.7	1,072	–64.1	—
31R-2, 106–111	692.86	43,191	16.0	2,612	–64.5	–191
50R-1, 129–134	783.89	20,091	10.5	1,595	–63.4	–187
52R-2, 0–5	795.30	23,381	10.4	1,821	–64.4	–195
344-U1412A-						
2H-6, 67–72	14.09	8,497	1.4	5,920	–79.0	–190
3H-3, 0–5	18.40	14,278	0.9	9,553	–81.3	–190
5H-4, 0–5	36.27	10,897	0.6	16,902	–68.9	–190
6H-3, 0–5	44.95	7,473	0.7	5,221	–62.2	–194
8H-2, 0–5	59.01	3,758	ND	—	–65.2	—
9H-7, 0–5	70.61	5,782	0.7	8,355	–67.5	–191
11H-3, 0–5	84.04	5,491	ND	—	–57.0	–188
14H-3, 0–5	98.33	4,850	0.8	5,857	–62.9	–194
17X-3, 0–5	115.94	6,519	1.0	6,552	–63.2	–187
18X-3, 0–5	125.41	4,582	1.3	3,597	–63.9	–186
20X-2, 0–5	143.60	5,071	1.3	3,957	–59.6	–186
22X-1, 0–5	162.76	7,067	1.8	3,868	–58.7	–191
24X-3, 0–5	182.59	26,846	3.1	8,765	–59.2	–191
344-U1412B-						
8X-1, 0–5	204.30	9,040	1.2	7,433	–60.7	–192
12X-1, 23–28	233.63	17,084	11.9	1,434	–63.8	–191
344-U1412C-						
2R-1, 109–114	301.09	1,573	1.2	1,307	–64.0	—
5R-1, 31–36	329.11	5,554	7.2	775	–62.3	–189
8R-6, 0–5	364.49	9,558	3.1	3,085	–60.0	–185
344-U1413A-						
4H-2, 0–5	27.03	10,793	ND	—	–69.9	–198
9H-3, 0–5	73.02	13,265	ND	—	–65.6	–193
10H-3, 0–5	82.43	13,989	ND	—	–67.2	–190
11H-3, 0–5	91.93	8,519	ND	9,734	–67.0	–189
12H-5, 0–5	103.50	6,983	ND	—	–64.4	–185
14H-4, 0–5	117.57	12,432	ND	—	–59.6	–185
18H-3, 0–5	138.64	9,704	0.5	18,725	–64.2	–181
20X-7, 0–5	157.47	3,484	0.6	5,833	–63.2	—
25X-2, 0–5	180.24	14,003	2.4	5,909	–71.7	–192
344-U1413C-						
7R-7, 0–5	234.78	3,343	2.5	1,318	–69.3	—
11R-2, 0–5	266.81	5,202	4.0	1,316	–60.4	—
20R-4, 0–5	356.07	8,448	21.0	298	–58.2	–195
23R-4, 0–5	386.04	6,801	15.6	310	–71.4	–202
31R-5, 0–5	464.61	3,693	19.1	148	–60.5	–195
36R-6, 0–5	514.43	4,097	74.2	50	–67.3	—
38R-5, 0–5	533.25	4,900	75.5	58	–60.4	–209
42R-3, 0–5	568.41	3,659	106.1	30	–64.6	–207

ND = no detection, — = no measurement.

Table T2. Molecular and isotopic compositions and conversion ratio of void gas, Sites U1412 and U1413.

Core, section, interval (cm)	Depth (mbsf)	Methane (ppmv)	Ethane (ppmv)	Propane (ppmv)	CO_2 (ppmv)	C_1/C_{2+}	$\delta^{13}C_{CH4}$ (‰)	δD_{CH4} (‰)	$\delta^{13}C_{CO2}$ (‰)	$\delta^{13}C_{org}$ (‰)	Conversion ratio
344-U1412A-											
4H-4, 50–51	29.93	819,908	16.4	1.6	5,187	45,669	–74.9	–190	–4.7	–23.8	23.8
5H-4, 50–51	36.77	822,693	16.4	1.6	4,612	45,663	–72.7	–189	–1.4	–23.8	26.9
6H-1, 50–51	42.50	773,388	14.2	1.0	1,703	50,841	–70.9	–189	0.3	–24.4	29.3
7H-1, 50–51	50.00	840,741	16.8	1.2	3,389	46,640	–70.2	–188	1.4	–24.5	30.4
9H-2, 50–51	64.87	834,864	29.6	1.0	4,436	27,255	–69.5	–189	0.8	–24.8	30.5
9H-7, 50–51	71.11	849,071	56.1	ND	1,908	15,156	–69.8	–193	–0.8	–23.6	28.2
11H-4, 50–51	85.75	849,076	28.0	2.7	2,571	27,603	–68.7	–187	0.8	–24.7	30.7
12H-2, 50–51	88.17	842,363	54.5	2.2	3,500	14,853	–68.9	–189	–0.5	–24.2	29.3
13H-4, 50–51	95.41	849,857	44.6	3.1	2,731	17,825	–68.7	–187	–1.5	–24.6	29.1
14H-3, 50–51	98.83	838,382	53.4	4.3	5,065	14,522	–68.5	–187	–0.3	–24.0	29.3
18X-3, 50–51	125.91	788,186	62.9	10.9	11,098	10,680	–67.0	–185	–0.2	–23.5	29.5
19X-2, 50–51	134.40	837,884	58.6	7.0	6,416	12,773	–67.0	–184	–1.5	–23.5	28.6
23X-4, 50–51	175.90	843,663	85.3	7.2	6,828	9,119	–66.9	–183	–3.4	–24.3	28.0
344-U1412B-											
6X-3, 50–51	187.50	845,587	28.4	0.6	5,358	29,207	–64.3	–189	–10.4	–24.2	22.6
7X-3, 50–51	196.74	850,241	46.7	2.9	8,708	17,135	–64.8	–188	–10.8	–24.1	21.8
344-U1413A-											
5H-3, 50–51	38.51	836,721	4.9	0.7	6,354	148,780	–71.6	–187	0.3	–23.5	28.2
6H-1, 50–51	45.10	836,575	3.9	1.8	3,613	146,487	–71.6	–187	–2.2	–25.0	27.9
7H-5, 50–51	58.24	841,035	4.0	4.4	4,601	99,270	–71.3	–187	–0.7	–25.0	29.1
8H-6, 50–51	68.56	830,880	4.2	5.0	5,182	90,938	–71.5	–187	–0.5	–26.0	30.2
9H-3, 50–51	73.52	833,201	3.8	4.4	4,202	100,554	–71.5	–186	–1.3	–25.3	28.9
10H-1, 50–51	80.00	821,828	5.0	5.9	7,683	76,004	–71.3	–185	–1.6	–24.9	28.4
11H-3, 50–51	92.43	792,361	4.4	4.7	506	87,704	–71.4	–186	–1.3	–25.8	29.5
13H-6, 10–11	112.59	825,058	6.9	7.2	4,722	58,668	–71.3	–185	–2.6	–23.6	26.4
14H-2, 50–51	115.16	829,723	6.6	5.9	1,874	65,943	–71.7	–185	—	–25.2	—
15H-3, 50–51	122.13	831,810	8.7	7.6	5,739	51,118	–72.0	–187	–2.8	–25.5	28.0
16H-4, 50–51	128.99	828,144	9.2	6.6	3,848	52,397	–72.3	–184	–3.6	–25.9	27.7
18H-2, 50–51	137.62	825,281	11.5	5.6	4,412	48,126	–73.0	–183	–3.8	–25.6	27.0

ND = no detection, — = no measurement.